Effects of the quark field on the ghost propagator of lattice Landau gauge QCD

Sadataka Furui[*]

School of Science and Engineering, Teikyo University, Utsunomiya 320-8551, Japan

Hideo Nakajima[†]

Department of Information Science, Utsunomiya University, Utsunomiya 321-8585, Japan

Infrared features of the ghost propagator of color-diagonal and color antisymmetric ghost propagator of quenched SU(2) and quenched SU(3) are compared with those of unquenched Kogut-Susskind fermion SU(3) lattice Landau gauge. We compare (i) the fluctuation of the ghost propagator, (ii) the ghost condensate parameter v of the local composite operator (LCO) approach, and (iii) the Binder cumulant of color antisymmetric ghost propagator between quenched and unquenched configurations. The color-diagonal SU(3) ghost dressing function of unquenched configurations has weaker singularity than the quenched configurations. In both cases fluctuations become large in $q < 0.5$ GeV. The ghost condensate parameter v in the ghost propagator of the unquenched MILC$_c$ configuration samples is ~ 0.002–0.04 GeV^2 while that of the SU(2) parallel tempering samples is consistent with 0. The Binder cumulant defined as $U(q) = 1 - \frac{1}{3} \frac{\langle \vec{\phi}^4 \rangle}{(\langle \vec{\phi}^2 \rangle)^2}$, where $\vec{\phi}(q)$ is the color antisymmetric ghost propagator measured by the sample average of gauge fixed configurations via parallel tempering method, becomes $\sim 4/9$ in all the momentum region. The Binder cumulant of the color antisymmetric ghost propagator of quenched SU(2) can be explained by the 3D Gaussian distribution, but that of the unquenched MILC$_c$ deviates slightly from that of the eight-dimensional Gaussian distribution. The stronger singularity and large fluctuation in the quenched configuration could be the cause of the deviation of the Kugo-Ojima confinement parameter c from 1, and the presence of ordering in the ghost propagator of unquenched configurations makes it closer to 1.

I. INTRODUCTION

Infrared features of the ghost propagator are important in the analysis of color confinement mechanism and the running coupling. Kugo and Ojima [1] considered the two point function connected by the ghost propagator and expressed the confinement criterion as

$$1 + u(0) = 1 - c = \frac{Z_1}{Z_3} = \frac{\tilde{Z}_1}{\tilde{Z}_3} = 0 \qquad (1)$$

at the renormalization point $\mu = 0$ [2]. Here Z_1 and $\tilde{Z}_1$ are the vertex renormalization factor of the triple gluon vertex and the ghost antighost gluon vertex, respectively, and Z_3 and $\tilde{Z}_3$ are the wave function renormalization factor of the gluon and the ghost, respectively.

If $\tilde{Z}_1$ is finite, divergence of $\tilde{Z}_3$ is a sufficient condition of the color confinement. The lattice data suggest that $\tilde{Z}_3$ is infrared divergent, but its singularity is not strong enough to hinder the running coupling, measured as

$$\alpha_s(q) = \frac{g_0^2}{4\pi} \frac{Z(q^2)G(q^2)^2}{\tilde{Z}_1^2} \sim \alpha_s(\Lambda_{UV}) q^{-2(\alpha_D + 2\alpha_G)}, \quad (2)$$

approach zero in the infrared [3]. Here $Z(q^2)$ and $G(q^2)$ are the gluon dressing function and the ghost dressing function, respectively. The same observation is reported in [4].

The ghost propagator in the infrared region was investigated by several authors. Common findings are that it is more singular than q^{-2} and that in the infrared region its statistical fluctuation is large probably due to the presence of Gribov copies [5–9]. In the quenched 32^4, 48^4, and 56^4 SU(3) lattice simulation, the color-diagonal ghost propagator showed singularity of $q^{-2-\alpha_G}$ with $\alpha_G \sim 0.25$. In the Dyson-Schwinger (DS) approach, the infrared power behavior of the ghost propagator and the gluon propagator $q^{-2-\alpha_D}$ have the relation $2\alpha_G + \alpha_D = 0$ and the lattice data are consistent with this ansatz in the $q > 1$ GeV region. As the magnitude of the α_D, the Dyson-Schwinger approach [10] and the Langevin approach [11] predict -0.59, while the lattice data and DS approaches [12,13] predict -0.5. If α_D is smaller than -0.5 the gluon propagator in the infrared vanishes and the Gribov-Zwanziger's conjecture on the color confinement of the gluon becomes satisfied. Recent detailed analysis of the finite size effect in the lattice confirms that the infrared limit of $-\alpha_D$ in the DS approach $\kappa = 0.5$ is compatible with the lattice data [14,15]. The relation $2\alpha_G + \alpha_D = 0$ suggests the presence of an infrared fixed point [10]. The infrared finite quark wave function renormalization Z_ψ of unquenched simulation [16] also suggests that the running coupling is not infrared vanishing.

---

*Electronic address: furui@umb.teikyo-u.ac.jp
URL: http://albert.umb.teikyo-u.ac.jp/furui_lab/furuipbs.htm
†Electronic address: nakajima@is.utsunomiya-u.ac.jp

We cannot measure the ghost propagator at zero momentum, since we evaluate it with the condition that it is zero-mode-less. Thus, the infrared power fitted at finite lattice momentum α_G cannot predict the power behavior of the ghost propagator near momentum 0, i.e. the index κ.

In [3], we observed that the Kugo-Ojima confinement criterion is satisfied in the unquenched simulation but not in the quenched simulation of lattice sizes up to 56^4. In order to study the role of the fermion in the color confinement, we consider the BRST (Becchi-Rouet-Stora-Tyutin) quartet mechanism [1,17].

In the BRST formulation [1], unphysical degrees of freedom are confined by the quartet mechanism. In the pure QCD in the Landau gauge, one can construct the BRST quartet as

$$A_\mu \to D_\mu(A)c \to 0 \qquad A_\mu \bar{c} \to D_\mu(A)c\bar{c} - A_\mu B \to 0.$$

Here the arrow implies the BRST transformation δ_B and B is the Nakanishi-Lautrup auxiliary field. The transverse gluon state A_μ is a BRST parent state of a daughter state $D_\mu(A)c$ and the state with opposite ghost number of the $D_\mu(A)c$, i.e. $A\bar{c}$ becomes a parent state, whose daughter and the above three states construct a quartet.

Inclusion of the fermion field ψ allows one to construct another BRST quartet as

$$\psi \to -\psi c \to 0 \qquad \psi\bar{c} \to -\psi c\bar{c} - \psi B \to 0.$$

The Dirac fermion state ψ is a BRST parent state of ψc and the state with opposite ghost number state of ψc is $\psi\bar{c}$, which becomes a parent state of the BRST partner that constructs a quartet.

Inclusion of the fermion gives more restriction on the degrees of freedom of the ghost and it may change the fluctuation of the ghost propagator.

Another current problem concerning the ghost propagator is the possibility of the ghost condensates. In the lattice Landau gauge QCD simulation, the presence of A^2 condensates was suggested [3,5–7,18]. Since A^2 is not BRST invariant, a mixed condensate, i.e. a combination with ghost condensates

$$\int \left\langle \mathrm{tr}_{G/H} \left[\frac{1}{2} \mathcal{A}_\mu \mathcal{A}^\mu - \xi i \mathcal{C}\bar{\mathcal{C}} \right] \right\rangle d^4 x, \qquad (3)$$

was proposed [19,20] as the on-shell BRST invariant, i.e. invariant for the B field that satisfies

$$B^a = -\frac{1}{\xi} \partial_\mu A^{a\mu} + i\frac{g}{2} f^{abc} c^b \bar{c}^c. \qquad (4)$$

Here G/H is the subset of gauge fixed configuration, and ξ is the gauge-fixing parameter. The Landau gauge $\xi = 0$ is regarded as a specific limit of the Curci-Ferrari gauge. In recent studies, the space-time average of the vacuum expectation value

$$\frac{1}{V} \int_V \left\langle \frac{1}{2} \mathrm{tr} \mathcal{A}_\mu(x) \mathcal{A}^\mu(x) \right\rangle d^4 x$$

is claimed to have gauge invariant meaning [19,21]. In the Landau gauge QCD, the Faddeev-Popov (FP) gauge-fixing action is

$$S_{\mathrm{FP}} = B^a \partial_\mu A^a_\mu + i\bar{\mathcal{C}}^a \partial_\mu D^{ab}_\mu \mathcal{C}^b, \qquad (5)$$

where the last term $\bar{C}^a \partial_\mu D_\mu{}^{ab} \mathcal{C}^b$, where $D^{ab}_\mu = \delta^{ab} \partial_\mu + g f^{acb} A^c_\mu$.

In analytical studies in the Curci-Ferrari gauge, presence of the ghost condensate $\langle f^{abc} c^b \bar{c}^c \rangle$ was discussed as the Overhauser effect in contrast to the $\langle f^{abc} c^b c^c \rangle$ or $\langle f^{abc} \bar{c}^b \bar{c}^c \rangle$ which are regarded as the BCS effect [22].

Since the Landau gauge is a specific limit of the Curci-Ferrari gauge, it is of interest to study the ghost propagator. In [6], we observed that in the SU(2) $\beta = 2.1$ 16^4 lattice, the expectation value of color off-diagonal ghost propagator $\langle \epsilon^{abc} \bar{c}^b c^c \rangle$ is consistent with 0 but the standard deviation of the color-diagonal ghost propagator has the momentum dependence of $\sigma(G^{aa}(q)) \propto q^{-4}$. The investigation was extended by [23] and this fluctuation was confirmed and, although the expectation value of $\phi^a(q) = \epsilon^{abc} c^b c^c$ is consistent with 0, the expectation value of its absolute value $|\phi^a(q)|$ was shown to behave as q^{-4} and not zero. We extend this approach to unquenched MILC configurations.

In [23], the ghost condensate parameter v and the Binder cumulant [24] of the color antisymmetric ghost propagator were measured. In the Binder cumulant of an order parameter, renormalization factors cancel and one can extract the fixed point in the continuum limit by a suitable extrapolation.

In the Zwanziger Lagrangian [25], the color antisymmetric ghost field $\phi^{bc}_\mu(x)$ leads to the mass gap equation

$$f^{abc} \langle A^{a\mu}(x) \phi^{bc}_\mu(x) \rangle = \frac{4(N_c^2 - 1)\gamma^2}{\sqrt{2} g^2}, \qquad (6)$$

where γ^2 is the mass dimension two Gribov mass parameter [26]. It is not evident that the Zwanziger Lagrangian expresses the effective theory of the lattice Landau gauge QCD, but analytical calculation of the ghost propagator in two loop [26] and the local composite operator approach [22,27] suggest hints for solving entanglements in the confinement problem.

In this paper we study the ghost propagator of quenched SU(2) $\beta = 2.2$ 16^4 lattice gauge fixed to the Landau gauge via the parallel tempering (PT) method [28] and investigate the Binder cumulant. We extend the study to unquenched SU(3), using the MILC$_c$ configurations [29].

Organization of the paper is as follows. In Sec. II, we show definitions of the color-diagonal and color antisymmetric ghost propagator on the lattice. In Sec. III, fluctuation of the ghost propagator of quenched and unquenched configurations are compared. In Sec. IV, we compare the

parameter v of the ghost condensates from the color antisymmetric ghost propagators of quenched SU(2) PT configurations and unquenched MILC$_c$ configurations. In Sec. V, the Binder cumulant of the color antisymmetric ghost propagator of the quenched SU(2) and unquenched SU(3) are compared. A summary and discussion are given in Sec. VI.

II. THE GHOST PROPAGATOR

The ghost propagator $D_G{}^{ab}(q^2)$ and the ghost dressing function $G^{ab}(q^2)$ is defined by the Fourier transform (FT) of the expectation value of the inverse Faddeev-Popov operator $\mathcal{M} = -\partial_\mu \mathcal{D}_\mu$

$$\text{FT}[D_G{}^{ab}(x, y)] = \text{FT}\langle\text{tr}(\Lambda^{a\dagger}\{(\mathcal{M}[U])^{-1}\}_{xy}\Lambda^b)\rangle$$

$$= D_G{}^{ab}(q^2) = \frac{G^{ab}(q^2)}{q^2} \qquad (7)$$

where anti-Hermitian SU(3) generator Λ^a is normalized as $\text{tr}\Lambda^{a\dagger}\Lambda^b = \delta^{ab}$.

We measure

$$D_G{}^{ab}(q^2) = \langle\text{tr}\langle\Lambda^a q|\mathcal{M}[U]^{-1}|\Lambda^b q\rangle\rangle \qquad (8)$$

using the source vector $|\Lambda^a q\rangle = \frac{1}{\sqrt{V}}\Lambda^a e^{iq\cdot x}$. We select the momentum q_μ to be directed along the diagonal of the lattice momentum space.

In the approach of calculating the Fourier transform of $\mathcal{M}^{-1}S_0^a(x)$ [5], compensation of hypercubic artifacts was necessary, but in our method the artifact-free momenta are selected and the translation invariance is fully utilized to improve the statistics.

The Faddeev-Popov operator $\mathcal{M}[U] = -\partial D[U]$ is defined with the use of the covariant derivative as

$$D_\mu(U_{x,\mu})\phi = S(U_{x,\mu})\partial_\mu\phi + [A_{x,\mu}, \bar{\phi}], \qquad (9)$$

where $\partial_\mu\phi = \phi(x+\mu) - \phi(x)$, $\bar{\phi} = \frac{1}{2}(\phi(x+\mu) + \phi(x))$. In the U-linear version, $[A_{x,\mu} = \frac{1}{2}(U_{x,\mu} - U_{x,\mu}^\dagger)|_{trlp}$ where $|_{trlp}$ means the traceless part] $S(U_{x,\mu})B_{x,\mu}$ is defined as

$$S(U_{x,\mu})B_{x,\mu} = \frac{1}{2}\left\{\frac{U_{x,\mu} + U_{x,\mu}^\dagger}{2}, B_{x,\mu}\right\}\Bigg|_{trlp} \qquad (10)$$

and in the $\log-U$ version, $(U_{x,\mu} = e^{A_{x,\mu}})$

$$S(U_{x,\mu})B_{x,\mu} = \frac{A_{x,\mu}}{2\tanh(A_{x,\mu}/2)}B_{x,\mu}, \qquad (11)$$

where $A_{x,\mu} = adjA_{x,\mu}$ [28].

In [23], the Faddeev-Popov operator was parametrized as

$$\mathcal{M}_U^{bc}(x, y) = \delta^{bc}\mathcal{S}(x, y) - f^{bcd}\mathcal{A}^d(x, y). \qquad (12)$$

The authors decomposed the inverse matrix $D_G{}^{bc}(x, y) = (\mathcal{M}^{-1})^{bc}(x, y)$ into $D_{G_e}{}^{bc}(x, y)$ and $D_{G_o}{}^{bc}(x, y)$, i.e. the

component containing even number of $\mathcal{A}$, odd number of $\mathcal{A}$, respectively. They derived the ghost propagator from $[\delta^{bc}/(N_c^2 - 1)]D_{G_e}{}^{bc}(x, y)$, and the color antisymmetric ghost propagator by multiplying $\mathcal{S}^{-1}\mathcal{A}$ to the color antisymmetric ghost propagator $D_{G_e}{}^{bc}(x, y)$ which contains the perturbation series of even numbers of $\mathcal{A}$.

We do not adopt this procedure, but derive directly the color antisymmetric ghost propagators by the conjugate gradient method. The convergence condition on the series is set to less than a few percent in the l_2 norm.

We define $\mathcal{M} = -\partial_\mu D_\mu$ and solve

$$-\partial_\mu D_\mu f_s^b(\mathbf{x}) = \frac{1}{\sqrt{V}}\Lambda^b \sin\mathbf{q}\cdot\mathbf{x} \qquad (13)$$

and

$$-\partial_\mu D_\mu f_c^b(\mathbf{x}) = \frac{1}{\sqrt{V}}\Lambda^b \cos\mathbf{q}\cdot\mathbf{x}. \qquad (14)$$

Then we calculate the overlap to get the color-diagonal ghost propagator

$$D_G(q) = \frac{1}{N_c^2 - 1}\frac{1}{V}\delta^{ab}(\langle\Lambda^a \cos\mathbf{q}\cdot\mathbf{x}|f_c^b(\mathbf{x})\rangle$$
$$+ \langle\Lambda^a \sin\mathbf{q}\cdot\mathbf{x}|f_s^b(\mathbf{x})\rangle) \qquad (15)$$

and color antisymmetric ghost propagator

$$\phi^c(q) = \frac{1}{\mathcal{N}}\frac{1}{V}f^{abc}(\langle\Lambda^a \cos\mathbf{q}\cdot\mathbf{x}|f_s^b(\mathbf{x})\rangle$$
$$- \langle\Lambda^a \sin\mathbf{q}\cdot\mathbf{x}|f_c^b(\mathbf{x})\rangle), \qquad (16)$$

where $\mathcal{N} = 2$ for SU(2) and 6 for SU(3).

III. FLUCTUATION OF THE GHOST PROPAGATOR

We present in the following subsections the square and the absolute value of the color antisymmetric ghost propagators of the quenched SU(2) $\beta = 2.2$ 16^4 lattice, and compare the corresponding values of the SU(2) Landau gauge QCD of larger samples [23]. We measure also ghost propagators of quenched SU(3) $\beta = 6.45$ 56^4 lattice and those of unquenched MILC$_c$ with lattice size $20^3 \times 64$ and MILC$_f$ with lattice size $28^3 \times 96$. We present the square and the absolute value of the color antisymmetric ghost propagator of MILC$_c$.

A. Quenched SU(2)

We select momenta q following the cylinder cut, and in the case of unquenched SU(3) $20^3 \times 64$ lattice calculation, it takes about 260 iterations in the $q = 0.2$ GeV region but several iterations in the $q = 4$ GeV region. The average of the color antisymmetric ghost propagator $\phi^c(q)$ is consistent with 0 but the average of its square $\phi^c(q)^2$ has a
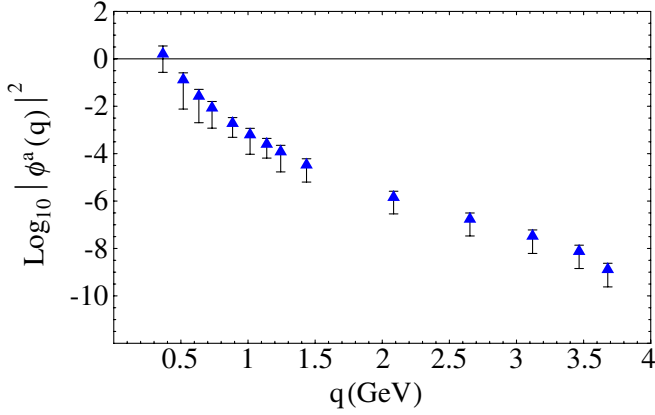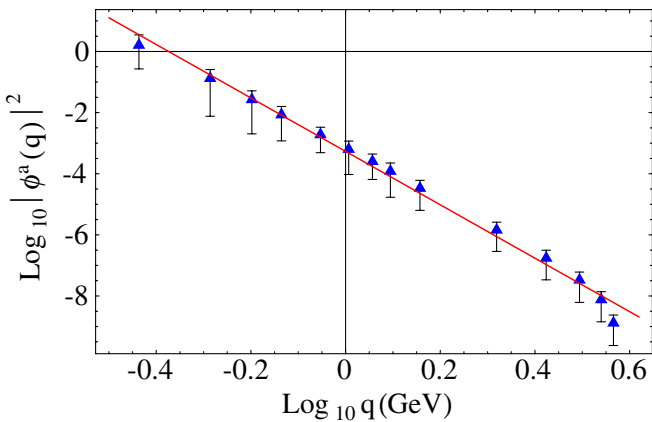
FIG. 1 (color online). Log of color antisymmetric ghost propagator squared $\log_{10}[\phi(q)^2]$ as the function of $q(\text{GeV})$. $\beta = 2.2$, 16^4 PT gauge fixing.

nonvanishing value. We define

$$\vec{\phi}(q)^2 = \frac{1}{N_c^2 - 1} \sum_c \phi^c(q)^2. \qquad (17)$$

The log of $\vec{\phi}(q)^2$ of $\beta = 2.2$ 16^4 lattice gauge fixed by the PT method (67 samples) is shown in Fig. 1. The corresponding log-log plots (Fig. 2) are to be compared with that of the ghost propagator $D_G(q)$ (Fig. 3).

The infrared singularity of the standard deviation of the color antisymmetric ghost dressing function and the color-diagonal ghost dressing function are $q^{-4.4}$ and $q^{-4.5}$, respectively.

B. Quenched SU(3)

In Fig. 4 we show the color-diagonal ghost propagator of quenched SU(3) with $\beta = 6.4$ ($1/a = 3.66$ GeV) and $\beta = 6.45$ ($1/a = 3.8697$ GeV) on 56^4 lattice. The corresponding ghost dressing function is in Fig. 5.

FIG. 2 (color online). Log of the color antisymmetric ghost propagator squared $\log_{10}[\phi(q)^2]$ as the function of $\log_{10}[q(\text{GeV})]$. $\beta = 2.2$, 16^4 PT gauge fixing.
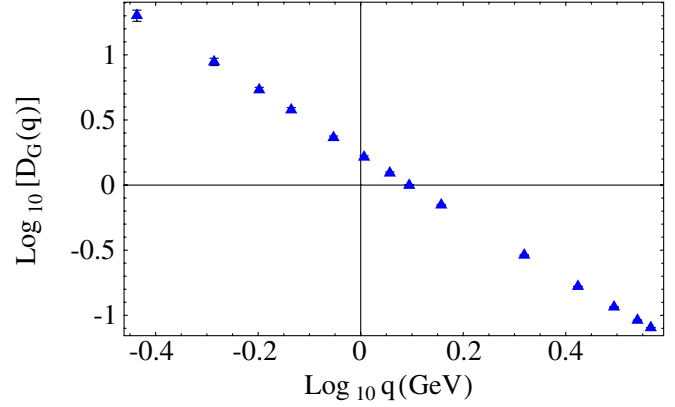

FIG. 3 (color online). Log of the ghost propagator $\log_{10}[D_G(q)]$ as the function of $\log_{10}[q(\text{GeV})]$. $\beta = 2.2$, 16^4 PT gauge fixing.

The standard deviation of the color-diagonal ghost propagator of $\beta = 6.45$ multiplied by $(qa)^4$ is almost constant in the $q > 1$ GeV region but in the $q < 0.5$ GeV region it is enhanced as compared to the value at the $q > 1$ GeV region.

The log-log plot of the standard deviation of the color-diagonal ghost dressing function of $\beta = 6.45$ in the $q < 1$ GeV region behaves as

$$\sigma(G(q)) \propto q^{-2.8(1)}. \qquad (18)$$

C. Unquenched SU(3)

In [7] we showed lattice results of the color-diagonal ghost dressing function of unquenched JLQCD/CP-PACS and MILC. In these simulations the length of the time axis is longer than the spacial axes and the ghost propagator of low momentum region is extended. In Fig. 6 the log-log plots of the ghost dressing function of the MILC$_f$ $\beta_{\text{imp}} = 7.09$ on $28^3 \times 96$ lattice and that of quenched $\beta = 6.45$ on
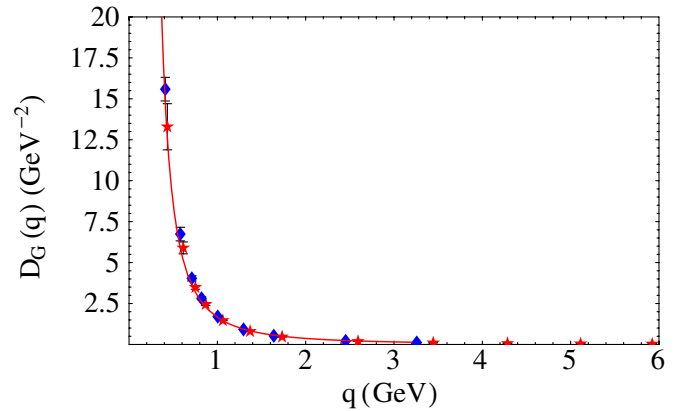

FIG. 4 (color online). The ghost propagator as the function of the momentum $q(\text{GeV})$. $\beta = 6.45$, 56^4 (stars) and $\beta = 6.4$, 56^4 (filled diamonds) in the $\log U$ definition. The solid line is the pQCD fit in $\widetilde{MOM}$ scheme [7].
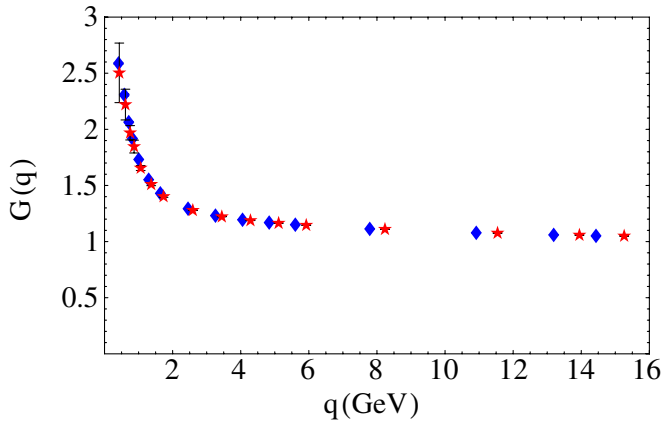
FIG. 5 (color online). The ghost dressing function as the function of the momentum q(GeV). $\beta = 6.45$, 56^4 (stars) and $\beta = 6.4$, 56^4 (filled diamonds) in the $\log - U$ definition.

FIG. 7 (color online). Log of the standard deviation $\log_{10} \sigma(G(q))$ as a function of $\log_{10} q$(GeV) of MILC$_f$ $\beta_{imp} = 7.09$ (upper points) and that of quenched $\beta = 6.45$ 56^4 (lower points).

56^4 lattice are shown. We observe suppression of the ghost propagator in the infrared region in the asymmetric lattice [3,18]. The systematic deviation of the ghost propagator and the gluon propagator of the asymmetric lattice from those of the symmetric lattice is recently confirmed in the large three-dimensional SU(2) lattice [30]. The suppression in the infrared of the unquenched data may not be due to the presence of quarks but due to the geometry of the lattice.

There are differences in the momentum dependence of the standard deviation of the color-diagonal ghost dressing function of unquenched MILC$_f$, $\beta_{imp} = 7.09$ on the $28^3 \times 96$ lattice and the quenched $\beta = 6.45$ on the 56^4 lattice in the infrared region as shown in Fig. 7. Since the sample size is different, the absolute value of the standard deviation is not meaningful, but the strength of the fluctuation defined by the slope influences the infrared behavior of the running coupling etc.
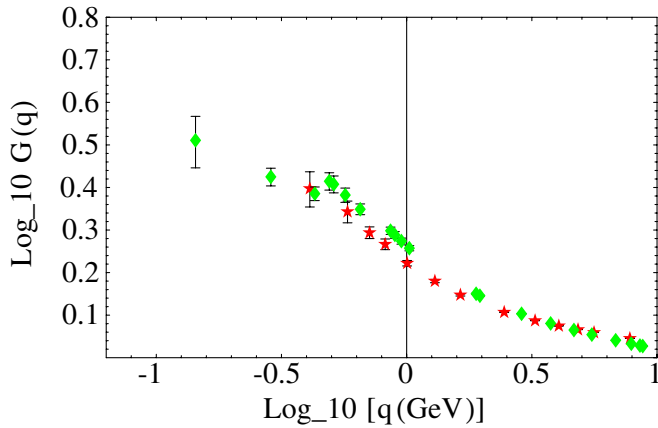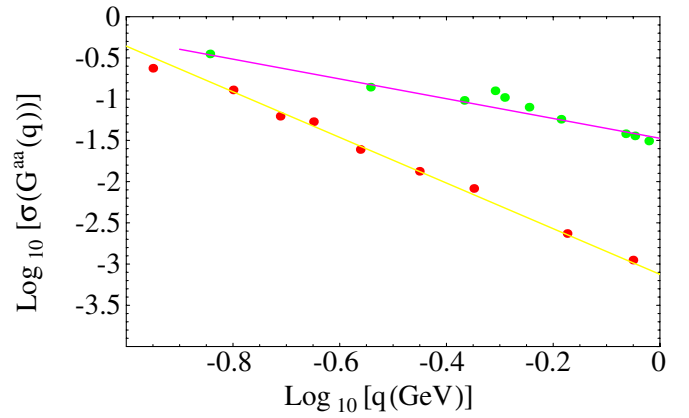
The momentum dependence of the standard deviation of the color-diagonal ghost dressing function of MILC$_f$ is dramatically less singular than that of the quenched configuration. We observed

$$\sigma(G(q)) \propto q^{-1.1(1)}. \qquad (19)$$

The color antisymmetric ghost propagator of MILC$_c$ (21 samples) is shown in Fig. 8. By comparing with Fig. 1, we observe a decrease of the slope.

IV. THE GHOST CONDENSATE

In the case of SU(2), the ghost condensate appears in the color antisymmetric ghost propagator $D_{G_o}{}^{bc}(q)$ related to $\phi^a(q)$ through

$$\phi^a(q) = -i \frac{f^{abc}}{2} D_G{}^{bc}(q^2) = -i \frac{f^{abc}}{2} D_{G_o}{}^{bc}(q) \qquad (20)$$
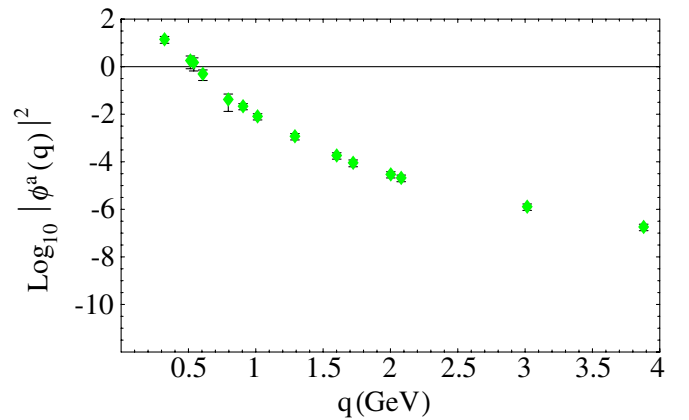
and

FIG. 6 (color online). Log of the ghost dressing function $\log_{10} G(q)$ as a function of $\log_{10} q$(GeV) of MILC$_f$ $\beta_{imp} = 7.09$ (diamonds) and that of quenched $\beta = 6.45$ 56^4 (stars).

FIG. 8 (color online). Log of the color antisymmetric ghost propagator squared $\log_{10}[\phi(q)^2]$ as the function of q(GeV). $\beta_{imp} = 6.83$, and 6.76, $20^3 \times 64$.
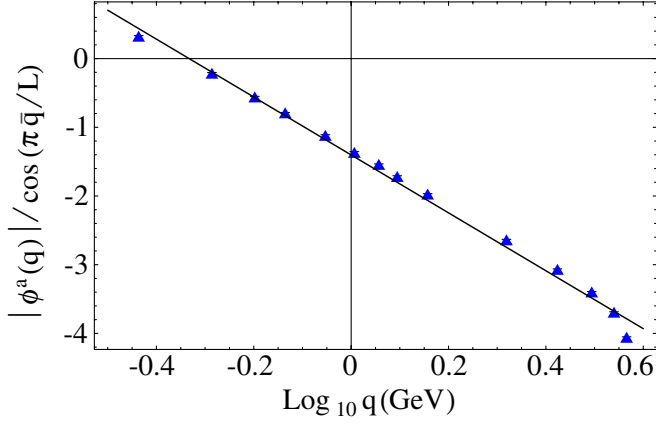
FIG. 9 (color online). Log of $|\phi^a(q)|$ (color antisymmetric ghost propagator) divided by $\cos(\pi\bar{q}a/L)$ as the function of $\log_{10}q$(GeV) of SU(2) PT samples.

$$D_{G_o}{}^{bc}(q) = i\frac{r/L^2 + v}{q^4 + v^2}\epsilon^{bc}, \tag{21}$$

where ϵ^{bc} is an antisymmetric tensor, i.e. when $a = 3$, b and $c = 1, 2$. In general, we parametrize the average of $|\phi^a(q)|$ as

$$\frac{1}{N_c^2 - 1}\sum_a |\phi^a(q)| = \frac{r/L^2 + v}{q^4 + v^2}. \tag{22}$$

Here L is the lattice size and the parameter r/L^2 is the correction from the finite size effect.

A. Quenched SU(2)

In [23], the fitting parameter r of $|\vec{\phi}^a(q)|$ (color antisymmetric ghost propagator) on the lattice was derived from
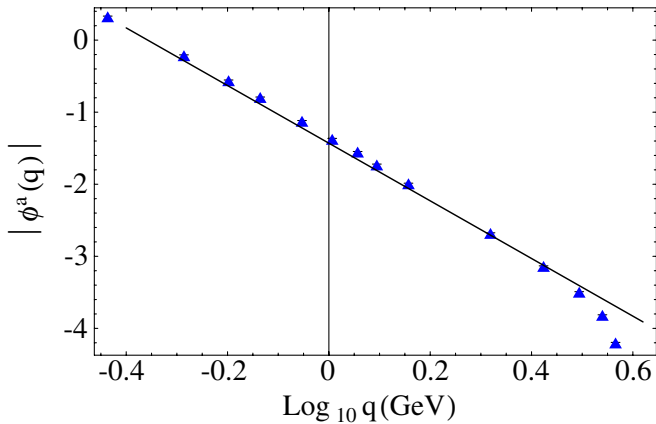

FIG. 10 (color online). Log of the absolute value $|\phi^a(q)|$ (color antisymmetric ghost propagator) as the function of $\log_{10}q$(GeV) of SU(2) PT samples.
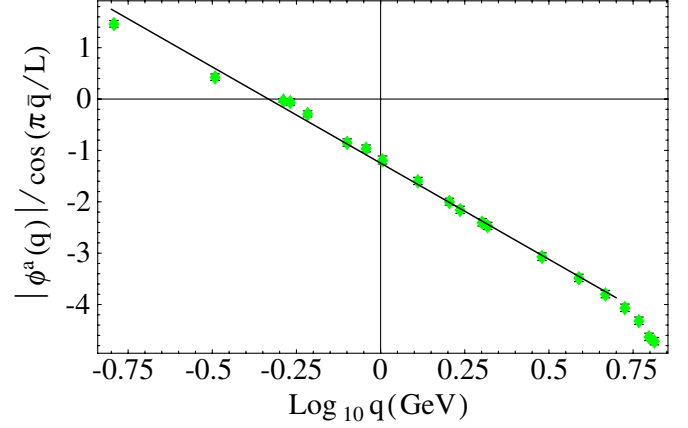

FIG. 11 (color online). Log of $|\vec{\phi}(q)|/\cos(\pi\bar{q}a/L)$ (color antisymmetric ghost propagator) as the function of $\log_{10}q$(GeV) of MILC$_c$ samples.

$$\frac{1}{3}\sum_a \frac{L^2}{\cos(\pi\bar{q}/L)}|\phi^a(q)| = \frac{r}{q^z}, \tag{23}$$

in which $\bar{q} = 0, 1, \ldots, L$.

Our fit of $\frac{|\phi^a(q)|}{\cos(\pi\bar{q}a/L)}$ of PT samples using $r = 10.13$, $z = 4.215$ is shown in Fig. 9.

Using $r = 10.13$, $L = 16$, the fitting parameter v of $|\phi(q)|$ is found to be -0.002 GeV^2 and is consistent with 0. The fit is shown in Fig. 10.

B. Unquenched SU(3)

As in the SU(2) PT samples, we performed the fit of the parameter v for the MILC$_c$ samples. We first fit the log of $|\phi^a(q)|$ (color antisymmetric ghost propagator) divided by $\cos(\pi\bar{q}a/L)$ using $L = \sqrt{20^3 \times 64}$ and obtained $r = 40.5$, $z = 3.75$, as shown in Fig. 11. The parameters r and z for the fit of $\vec{\phi}^2(q)/\cos^2(\pi\bar{q}/L)$ are $r = 36.5$, $z = 7.5$.
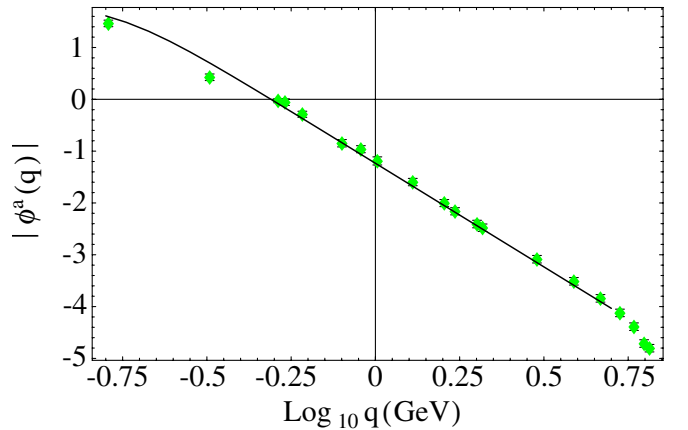

FIG. 12 (color online). Log of the absolute value $|\vec{\phi}(q)|$ (color antisymmetric ghost propagator) as the function of $\log_{10}q$(GeV) of MILC$_c$ samples.
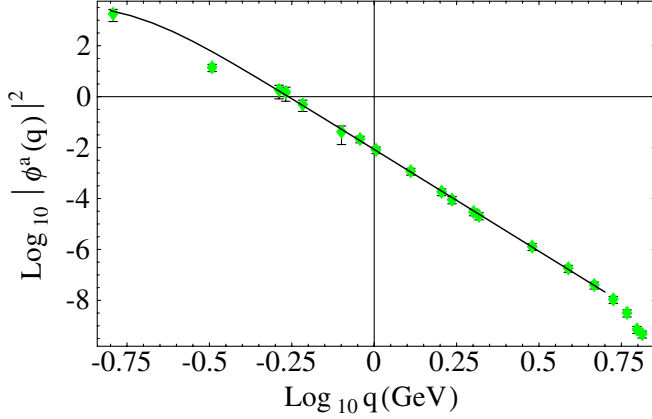
FIG. 13 (color online).   Log of the $\vec{\phi}(q)^2$ (color antisymmetric ghost propagator squared) as the function of $\log_{10}q$(GeV) of $MILC_c$ samples.

Our fit of $|\phi(q)|$ ignoring the two lowest momentum points and using $r = 40.51$ gives $v = 0.0020$ GeV^2, which is small but positive. When the two lowest momentum points are included, v decreases to -0.0005 but χ^2/d.o.f. increases. The former fit is shown in Fig. 12.

We fitted also $\log_{10}\vec{\phi}^2(q)$, where

$$\vec{\phi}^{\,2}(q) = \frac{1}{N_c^2 - 1}\sum_a \phi^a(q)^2 = \left(\frac{r/L^2 + v}{q^4 + v^2}\right)^2. \qquad (24)$$

The fit with $r = 40.5$, $v = 0.035$ GeV^2 is shown in Fig. 13. The fit with $r = 36.5$, $v = 0.041$ GeV^2 is not distinguished from this figure.

V. BINDER CUMULANT

Two decades ago, Binder [24] showed cumulants of the order parameter yields nontrivial fixed-point values. The theory was applied to the Ising model in which the magnetization M is the order parameter [31,32] and the cumulant was defined as

$$B = \frac{1}{2}\left(3 - \frac{\langle M^4 \rangle}{\langle M^2 \rangle^2}\right). \qquad (25)$$

When the distribution of M is given by the one-dimensional Gaussian distribution, one finds

$$\frac{\langle M^4 \rangle}{\langle M^2 \rangle^2} = 3 \qquad (26)$$

and B becomes 0.

In SU(2) and SU(3) lattice QCD, deconfinement phase transition was studied by measuring

$$g = \frac{\langle P^4 \rangle}{\langle P^2 \rangle^2} - 3 \qquad (27)$$

using the Polyakov line data P as the order parameter [33,34].

Since the color antisymmetric ghost propagator could be an order parameter of the system, the authors of [23] considered its Binder cumulant defined as

$$U(q) = 1 - \frac{\langle \vec{\phi}(q)^4 \rangle}{3\langle \vec{\phi}(q)^2 \rangle^2}. \qquad (28)$$

We measure

$$
\begin{aligned}
\vec{\phi}(q)^2 = \frac{1}{N_c^2 - 1}\sum_a\Bigg[\frac{1}{\mathcal{N}} \\
\times \frac{f^{abc}}{V}(\langle \Lambda^b \cos\mathbf{q}\cdot\mathbf{x}|\mathcal{M}^{-1}|\Lambda^c \sin\mathbf{q}\cdot\mathbf{x}\rangle \\
- \langle \Lambda^b \sin\mathbf{q}\cdot\mathbf{x}|\mathcal{M}^{-1}|\Lambda^c \cos\mathbf{q}\cdot\mathbf{x}\rangle)\Bigg]^2
\end{aligned}
\qquad (29)
$$

and

$$
\begin{aligned}
\vec{\phi}(q)^4 = \Bigg(\frac{1}{N_c^2 - 1}\sum_a\Bigg[\frac{1}{\mathcal{N}} \\
\times \frac{f^{abc}}{V}(\langle \Lambda^b \cos\mathbf{q}\cdot\mathbf{x}|\mathcal{M}^{-1}|\Lambda^c \sin\mathbf{q}\cdot\mathbf{x}\rangle \\
- \langle \Lambda^b \sin\mathbf{q}\cdot\mathbf{x}|\mathcal{M}^{-1}|\Lambda^c \cos\mathbf{q}\cdot\mathbf{x}\rangle)\Bigg]^2\Bigg)^2.
\end{aligned}
\qquad (30)
$$

In arbitrary d-dimensional space, corresponding expectation value for d-dimensional Gaussian distribution becomes

$$\frac{\langle \vec{\phi}^4 \rangle}{\langle \vec{\phi}^2 \rangle^2} = \frac{d + 2}{d}. \qquad (31)$$

Thus a natural extension to d-dimensional vector variable is

$$\tilde{U}(q) = \frac{\langle \vec{\phi}^4 \rangle}{\langle \vec{\phi}^2 \rangle^2} - \frac{d + 2}{d} \qquad (32)$$

which becomes 0 in the system with Gaussian distribution whose symmetry is not broken.

When the symmetry of the system is broken, as in the Ising model at the 0 temperature, the ratio of $\langle \vec{\phi}(q)^2 \rangle^2$ and $\langle \vec{\phi}(q)^4 \rangle$ becomes 1 and $\tilde{U}(q)$ becomes $-\frac{2}{d}$. It corresponds to the 0 temperature fixed point.

A. Quenched SU(2)

We measure the Binder cumulant $U(q)$ of the quenched SU(2) 16^4 $\beta = 2.2$, $a = 1.07$ GeV^{-1} configurations (67 samples) produced by the PT Landau gauge fixing and the corresponding first copy [6,28]. The q dependence of the $U(q)$ of PT gauge fixed samples and the first copies are shown in Fig. 14. The infrared fluctuation is large in the first copy but it is reduced in the PT gauge fixed samples. It implies a Gribov copy effect in the infrared region [8]. The average over $q > 0.5$ GeV becomes $U(q) = 0.45(2)$. This value is comparable to that of [23] obtained by 10 000 samples using symmetric momentum $q_1 = q_2 = q_3 = q_4 \neq 0$. In [23], the value $U(q)$ between 0 and 2/3 was interpreted as a system deviating from the Gaussian distri-
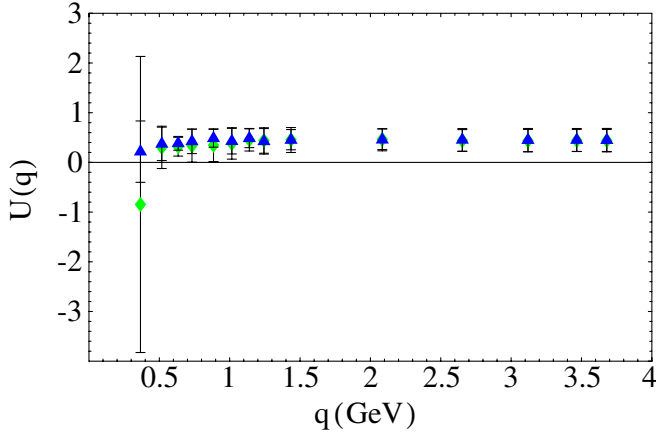
FIG. 14 (color online). The momentum dependence of Binder cumulant $U(q)$ of SU(2), $\beta = 2.2$, $a = 1.07$ GeV^{-1} of PT samples and first copy samples.

bution. However, since $\vec{\phi}(q)$ is a three-dimensional vector, it would not be appropriate to treat it as a one-dimensional object. The value 0.45 is very close to

$$U(q) \sim 1 - \frac{d+2}{3d} = \frac{4}{9}, \tag{33}$$

or

$$\tilde{U}(q) \sim \frac{5}{3} - \frac{d+2}{d} = 0 \tag{34}$$

corresponding to the 3D Gaussian distribution.

B. Unquenched SU(3)

We measured the Binder cumulant of the color antisymmetric ghost propagator of MILC$_c$. We observed qualitatively different features from quenched SU(2). An average of 9 $\beta_{\text{imp}} = 6.76$ samples and 12 $\beta_{\text{imp}} = 6.83$ samples of MILC$_c$ is shown in Fig. 15. When the $\vec{\phi}$ is distributed as a Gaussian vector in eight-dimensional space, $U(q) = 1 -$
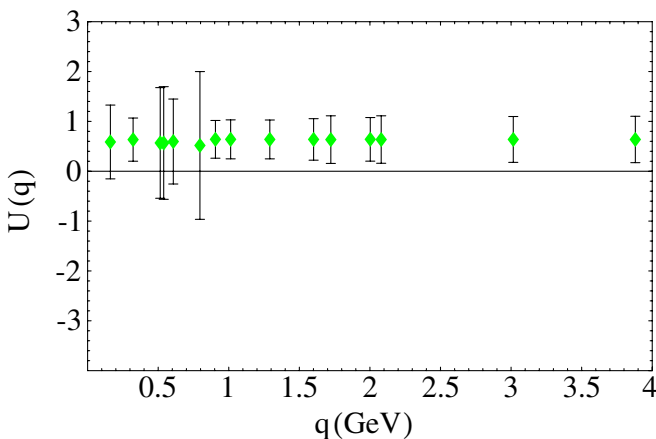

FIG. 15 (color online). The momentum dependence of Binder cumulant $U(q)$ of unquenched SU(3), $\beta_{\text{imp}} = 6.83$ and 6.76, $a = 1.64$ GeV^{-1} MILC$_c$.

$\frac{10}{3 \cdot 8} = 0.58$. Data of Fig. 15 suggest that $U(q)$ is slightly larger than the 0.58, and that the shift from Gaussian distribution of $\beta_{\text{imp}} = 6.76$ samples with light bare quark mass $m_0 = 11.5$ MeV is larger than that of $\beta_{\text{imp}} = 6.83$ samples with heavier bare quark mass $m_0 = 65.7$ MeV.

A qualitative difference of unquenched SU(3) (Fig. 15) from quenched SU(2) (Fig. 14) is the smallness of the fluctuation at the lowest and next to the lowest momentum point [$q = (0, 0, 0, 1)$ and $(0,0,0,2)$]. Relatively large fluctuation exists when one of the spacial components of q is 1 and other components are 0. The difference from the quenched SU(2) could be due to the improvement in the Asqtad action used in the MILC$_c$ and/or the presence of dynamical fermions.

VI. SUMMARY AND DISCUSSION

We presented the color-diagonal ghost propagator of quenched $\beta = 6.45$ 56^4 lattice and those of unquenched MILC$_c 20^3 \times 64$ and MILC$_f 28^3 \times 96$ configurations. The momentum dependence of standard deviation of the color-diagonal ghost dressing function of the unquenched configurations is less singular than that of the quenched configurations. The standard deviation and the mean value of statistical distribution is important for determining the nature of the ensemble.

The ghost pair creation operator in the BCS channel is expected to behave as the order parameter, and in the Landau gauge, where ghost pair creation is absent, the ghost antighost pair creation in the Overhauser channel was speculated to become an order parameter. The parameter v of LCO approach that characterizes the ghost condensate was compatible with 0 in the SU(2) PT samples. In the unquenched SU(3) MILC$_c$ samples, we found a small but positive value of v. Uncertainty on v comes mainly from that of r, where finite size effect is crucial. We need to extend the analysis to larger lattices to get the definite conclusion.

We showed that the Binder cumulant which measures the fluctuation of the ghost propagator differs between quenched and unquenched configurations. We confirmed that the Binder cumulant $U(q)$ of the color antisymmetric ghost propagator of SU(2) obtained by 10 000 samples [23] $U(q) \sim \frac{4}{9}$ is consistent with that obtained by using PT gauge fixed samples. In three-dimensional system, this data can be interpreted as $\tilde{U}(q)$ defined as Eq. (34) ~0, i.e. the color symmetry is not broken and that the system is in the random phase. When the system is ordered, a certain direction in the color space will be selected and the Binder cumulant would deviate from the value expected by the Gaussian distribution. The data of quenched SU(2) $\beta = 2.2$ do not show this tendency but the unquenched SU(3) show a slight deviation from the Gaussian distribution. Whether it implies the precursor of the ghost condensation in the unquenched QCD is not evident. It would be inter-

esting to extend the analysis to finite temperature and study qualitative differences.

The ghost condensates and the A^2 condensates are expected to be related by the on-shell BRST symmetry. The observables of lattice Landau gauge in the 1–3 GeV region suggest the presence of A^2 condensates. The larger standard deviation of the SU(3) quenched ghost propagator as compared to the unquenched ghost propagator may imply that the ghost propagator is more random in the quenched samples. The fluctuation of the ghost propagator could be the main cause of suppression of the running coupling in the infrared and saturation of the Kugo-Ojima parameter c at about 0.8 in the quenched approximation. It is likely that the fermion field reduces the fluctuation of the color-diagonal ghost propagator in the infrared, and renders the Kugo-Ojima parameter c close to 1.

We think infrared suppression of the running coupling of unquenched SU(3) measured by Eq. (2) presented in [3] is a finite size effect. In the process of measuring the ghost propagator for the running coupling, we observed large fluctuations of the norm and random orientation of the vector in adjoint color space, i.e. weakening of the color-diagonal structure of the ghost propagator in the infrared. Concerning the fixed points of the running coupling, Wilson [35] noted in 1971 that the renormalization group flow of the coupling could approach limit cycles which are more elaborate than simple isolated fixed points. A possibility of complicated fractal structure in fixed points was discussed in [36]. The Zamolodchikov's c-theorem in two-dimensional conformal field theory [37], however, excludes the limit cycle structure of the infrared fixed points. In four-dimensional QCD, the situation is obscure [38]. To clarify the nature of the infrared fixed points, it is necessary to investigate the continuum limit of the lattice Landau gauge QCD via systematic studies of finite size effects and the Gribov copy effects.

ACKNOWLEDGMENTS

[1] T. Kugo and I. Ojima, Prog. Theor. Phys. (Kyoto) Suppl. **66**, 1 (1979).
[2] T. Kugo, hep-th/9511033.
[3] S. Furui and H. Nakajima, hep-lat/0503029.
[4] E.-M. Ilgenfritz, M. Müller-Preussker, and A. Sternbeck, hep-lat/0601027.
[5] Ph. Boucaud, J. P. Leroy, A. Le Yaouanc, A. Y. Lokhov, J. Michelli, O. Pène, J. Rodríguez-Quintero, and C. Roiesnel, hep-lat/0506031.
[6] S. Furui and H. Nakajima, Phys. Rev. D **69**, 074505 (2004).
[7] S. Furui and H. Nakajima, Phys. Rev. D **70**, 094504 (2004).
[8] A. Sternbeck, E.-M. Ilgenfritz, M. Müller-Preussker, and A. Schiller, Phys. Rev. D **72**, 014507 (2005).
[9] J. C. R. Bloch, A. Cucchieri, K. Langfeld, and T. Mendes, Nucl. Phys. **B687**, 76 (2004).
[10] C. Lerche and L. von Smekal, Phys. Rev. D **65**, 125006 (2002).
[11] D. Zwanziger, Phys. Rev. D **69**, 016002 (2004).
[12] J. C. R. Bloch, Few-Body Syst. **33**, 111 (2003).
[13] K-I. Kondo, hep-th/0303251.
[14] Ph. Boucaud *et al.*, hep-lat/0602006.
[15] O. Oliveira and P. J. Silva, Proc. Sci., LAT2005 (2005) 287 [hep-lat/0509037]; [hep-lat/0511043].
[16] S. Furui and H. Nakajima, Phys. Rev. D **73**, 074503 (2006).
[17] R. Alkofer, W. Detmold, C. S. Fischer, and P. Maris, Phys. Rev. D **70**, 014014 (2004).
[18] S. Furui and H. Nakajima, Proc. Sci., LAT2005 (2005) 291 [hep-lat/0509035].

[19] K.-I. Kondo, Phys. Lett. B **619**, 377 (2005).
[20] B. M. Gripaios, Phys. Lett. B **558**, 250 (2003).
[21] A. A. Slavnov, Phys. Lett. B **608**, 171 (2005).
[22] D. Dudal, H. Verschelde, V. E. R. Lemes, M. S. Sarandy, S. P. Sorella, M. Picariello, A. Vicini, and J. A. Gracey, J. High Energy Phys. 06 (2003) 003.
[23] A. Cucchieri, T. Mendes, and A. Mihara, Phys. Rev. D **72**, 094505 (2005).
[24] K. Binder, Phys. Rev. Lett. **47**, 693 (1981).
[25] D. Zwanziger, Nucl. Phys. **B399**, 477 (1993).
[26] J. A. Gracey, Phys. Lett. B **632**, 282 (2006).
[27] M. A. L. Capri, D. Dudal, J. A. Gracey, V. E. R. Lemes, R. F. Sobreiro, S. P. Sorella, and H. Verschelde, Phys. Rev. D **73**, 014001 (2006).
[28] H. Nakajima and S. Furui, Nucl. Phys. B, Proc. Suppl. **141**, 34 (2005).
[29] C. Bernard *et al.*, Phys. Rev. D **58**, 014503 (1998).
[30] A. Cucchieri and T. Mendes, Phys. Rev. D **73**, 071502 (2006).
[31] G. Parisi and J. J.Ruiz-Lorenzo, Phys. Rev. B **54**, R3698 (1996).
[32] M. N. Barber, R. B. Pearson, D. Toussaint, and J. L. Richardson, Phys. Rev. B **32**, 1720 (1985).
[33] N. A. Alves, B. A. Berg, and S. Sanielevici, Nucl. Phys. **B376**, 218 (1992).
[34] J. Fingberg, U. Heller, and F. Karsch, Nucl. Phys. **B392**, 493 (1993).
[35] K. G. Wilson, Phys. Rev. D **3**, 1818 (1971).
[36] A. Morozof and A. J. Niemi, Nucl. Phys. **B666**, 311 (2003).
[37] A. B. Zamolodchikov, Sov. J. Nucl. Phys. **46**, 1090 (1987).
[38] J. L. Cardy, Phys. Lett. B **215**, 749 (1988).